LODZ UNIVERSITY OF TECHNOLOGY

FACULTY OF MECHANICAL ENGINEERING

DEPARTMENT OF DYNAMICS

inż. Marcin Kapitaniak
170332

MASTER OF SCIENCE THESIS

Mechatronics: Mechatronics in machine drives

Full-time studies

SYNCHRONOUS MOTION OF TWO VERTICALLY EXCITED PLANAR ELASTIC PENDULA

supervisor:
dr hab. inż. Przemysław Perlikowski

Contents

Chapter 1

Introduction

This thesis presents the analysis of the dynamics of two coupled elastic pendula, with particular attention to possible synchronous solutions. The analyzed system of two elastic pendula mounted on the oscillator, is subjected to parametric vertical periodic excitation. The thesis starts with the summary of the research perfomed in the field of dynamics of elastic pendula, including planar pendula (as in this thesis) and three-dimensional one. As a next step the different classification of synchronization phenomenon is provided. The thesis continues then with the detailed description of the analyzed system and the derivation of equations of motion with Lagrangian mechanics. The chapter describing the performed analysis, starts with the description of free oscillations, that allowed to observe synchronization, with net force acting on the oscillator mass equal to 0. The main part of the thesis concentrates on calculation of synchronization regions for both oscillatory and rotational solutions, which is done using numerical continuation. Finally the work considers in detail some asynchronous solutions that bifurcate from the observed synchronized solutions.

1.1 Elastic pendula literature review

The elastic pendulum is a simple mechanical system that exhibits a wide and surprising range of highly complex dynamic phenomena. There was some research in this area, with different approaches to the problem including classical perturbation techniques, that allow to obtain analytical solution, for ranges of parameters when motion is regular. The first known study of the elastic pendulum has been done by Vitt and Gorelik [18]. They considered a single two degree of freedom elastic pendulum, confined to a plane. The

equations of motion are derived from Lagrangian formulation. Cubic order terms are neglected, what is the consequence of assuming that amplitudes are sufficiently small. Two different linear modes are defined for oscillating pendulum mass and for pendula itself. Vitt and Gorelik considers a special case, for which the frequency of pendulum mass is twice the frequency of the pendulum. As a result both modes of motion can be induced by one another, through nonlinear interactions, that provide coupling between them. Such behaviour is known as a parametric resonance, in which the transfer of energy between the two components of the system takes place and depends strongly on applied initial conditions.

The studies of the system are based on secular perturbation theory. The authors compute periodic solutions, for two cases, with and without energy transfer between the components of the system. Either of these cases is ensured by application of appropriate initial conditions. As for the case without energy, the coupling is responsible only for changinig the frequencies of oscillations of the pendula and pendula masses, but preserving the 2:1 ratio between them. Periodic solutions, for which there is continuous exchange of energy between the components are obtained using perturbed Hamiltonian.

In addition to theoretical studies, Vitt and Gorelik perform experiments, which appear to be in good agreement with theoretical predictions. The authors pay particular attention to the strong dependence of nonlinear interactions between the possible modes of motion, on initial conditions. Finally the paper compares the observed parametric resonance with the quantum mechanical phenomenon of Fermi resonance, observed in the line spectrum of CO_2 molecule, for which the frequency ratio is close to 2:1, making both these behaviours closely analogous.

Lynch [7] generalized the results obtained by Vitt and Gorelik, by analyzing the three dimensional elastic pendulum. The equations of motion are derived similarly from Lagrange approach. Terms of higher than cubic order are neglected from the equations of motion. The author considers, as Vitt and Gorelik, two types of solutions with and without transfer of energy. Using perturbation theory, the paper considers conical motion of elastic pendulum. When the ratio between the natural frequencies of pendulum mass and pendulum is 2:1, resonance is observed, for which energy is periodically transferred between the components of the system. The approximate expressions describing the behaviour of 3D elastic pendulum are compared to numerical results, proving the usefullness of the proposed approach.

Lynch [8] gives an overview of the research performed for the system of 2D elastic pen-

dulum and shows how this simple system can be used to model the behaviour of the atmosphere. Due to the presence of coupling in the system, the analytical approach cannot be applied. Instead the author uses, as in Lynch [7] perturbation theory to compute solutions, where perturbation parameter ϵ describes the ratio of the frequencies for slow and fast oscillations. As a next step the Kolmogorov-Arnold-Moser (KAM) theorem is applied to ensure necessary restraints on the nature of the solutions. The validity of this approach is verified with the numerical results.

The system of elastic pendulum aroused much interest due to rich variety of solutions that are available. When the amplitudes of oscillations are small, the motion of the system is regular, and thus classical perturbation theory yields valid results. For bigger amplitudes the system enters chaotic regime, which covers the more phase-space, the more energy grows. As described by Nunez-Yepez *et al.* [11], for large energies, the motion of the pendulum becomes once more regular and predictable. In this paper, the authors used Hamiltonian approach to write equations of motion for the elastic pendulum and concentrated on chaotic motion. Like Vitt and Gorelik and Lynch, the behaviour of pendulum at parametric resonance 2:1 is studied. The authors demonstrate that for increased pendulum energy, the motion alternates between regular and chaotic one. Repeating transitions order-chaos-order are being observed for increased energy, whereas for small energies quasi-periodic solutions dominate. For large energies the pendulum rotates around suspension point in a regular manner, what means that for certain value of energy chaos starts to dissappear. It is explained that the motion becomes regular, because the observed rotational motion nullifies the strong nonlinear coupling between the components of the pendulum.

Davidovic *et al.*[5] studied also the elastic pendulum in resonance, but concentrated the attention at determining the limits of oscillatory motion of the pendulum and pendulum mass. The analysis is done using Hamiltonian approach, for the elastic pendulum described by parabolic coordinates.

Anicin *et al.* [1] considered the stability of elastic pendulum, by means of linear theory. As in other studies the ratio between the natural frequencies of pendulum mass and pendulum was 2:1. In this example the pendulum mass was forced harmonically. The authors aimed to determine graphically the parameters range, for which the instability of the initial vertical motion of the pendulum mass takes place and leads to oscillations of the pendulum via parametric resonance. This is achieved by writing the equation of motion for horizonthal direction in the form:

$$\ddot{x} + [\omega_1^2 + \beta A \cos(\omega_2 t)]x = 0 \tag{1.1}$$

where ω_1 denotes natural frequency of the pendulum, ω_2 is natural frequency of pendulum mass, A is amplitude of forcing, and $\beta = \omega_2^2 - \omega_1^2$ and comparing it with standard form of Matthieu equation:

$$\frac{\mathrm{d}^2 x}{\mathrm{d}\tau^2} + [a + 16q \cos(2\tau)]x = 0 \tag{1.2}$$

The stability is determined graphically using Ince-Strutt stability chart, what makes it possible to determine the range of pendulum masses that result in instability in the motion of the pendulum.

1.2   Synchronization

Synchronization is a very important phenomenon, observed in dynamical systems, especially the one containing pendula. Its name comes from Greek and means something that shares the same time. Synchronization was first observed in seventeenth century, by Huygens in the system of clocks placed on the ship on the open sea. These clocks were swinging in opposite directions, so this was the first example of exact synchronization. The clocks, when disturbed, still returned to the synchronous state, after some time, which was the result of their coupling through the beam on which the clocks were mounted.

By synchronization we understand adjustment of rhythms of self-sustained periodic oscillators, which result from weak interaction between them. According to Blekhman, (1988) this phenomenon can be described in terms of phase locking and frequency entrainment. Synchronization can be observed in rotator systems as well as in chaotic systems. When large number of systems are coupled together, the synchronization appear via non-equilibrium phase transitions.

It is possible to encounter synchronization in a group of non-coupled autonomous oscillators, subjected to periodic forcing or noise. This feature has many applications which include for example radio-controlled clocks, for which a periodic radio signal adjusts relatively non-precise clocks [13] and cardiac pacemakers where heart beats are paced by a sequence of pulses from an electronic generator [15]. For these cases the group of non-coupled oscillators is subjected to periodic forcing $f(t)$, which can lead, after the decay of the transient, to consistence of the vector states of the analyzed systems. It is neccessary for all conditional Lyapunov exponents to be negative, in order to observe synchronized solutions.

The presence of synchronization in dynamical system indicates that the responses of

its components are related to each other. In most cases this relationship is a complex one, therby making it more difficult to detect, since it is not always associated with both trajectories being the same. The classification of synchronization is based on relationship between the responses as desribed by [2]. Assuming we have two systems, described by their trajectories $x(t)$ and $y(t)$ respectively, we distinguish: complete synchronization [CS], phase synchronization [PS], lag synchronization [LS] and generalized synchronization [GS]. In case of *complete synchronization*, both phases and amplitudes of the oscillating systems have to coincide. In order to observe this state of synchronization the analyzed oscillators need to be identical, and either internal or external coupling between them has to be provided. According to Pecora and Caroll [12], for complete synchronization, phase trajectories $x(t)$ and $y(t)$ of the coupled systems converge to the same value and remain in this relation during the further time evolution. This can be described by:

$$\lim_{t \to \infty} |x(t) - y(t)| = 0, \tag{1.3}$$

Very often the above synchronization condition is not fulfilled completely. It is the result of presence of noise or small difference in parameters, and is known as *imperfect complete synchronization* [ICS], for which the synchronization condition is written as:

$$\lim_{t \to \infty} |x(t) - y(t)| = \epsilon, \tag{1.4}$$

where ϵ is a small parameter.

In nonidentical systems we can observe *phase synchronization* [PS], for which phases of oscillations are locked within a certain range. In that case a much weaker coupling is required, compared to the complete synchronization. The correlation between the phases doesn't usually result in any correlation between the amplitudes of oscillations. The condition describing phase synchronization is written as:

$$|n\Phi_1(t) - m\Phi_2(t)| < c, \tag{1.5}$$

where $\Phi_1(t)$ and $\Phi_2(t)$ are phases of coupled oscillators, ans m and n are constants describing locking ratio. As a result of the above condition, the frequencies of both oscillators have to be locked and fulfill:

$$n\omega_1 - m\omega_2 = 0, \tag{1.6}$$

Another possible type of synchronization is *lag synchronization* [LG], for which there appears a difference between the response of one system and the delayed response of the other system. Moreover this difference is bounded. It can be said that the one system anticipates the response of the second one. Both system appear to behave in the same

way, but their responses are shifted in time with respect to each other. The observed shift is know as the *lag time*. As a result for lag synchronization there is a relation between both phases and amplitudes of the two oscillating systems. If in the analyzed system we observe the state for which we have lag synchronization most of the time, but which is broken with intervals of asynchronous motion, we deal with *intermittent lag synchronization* [ILS].

If we analyze nonidentical oscillators and observe that the state of one system can be predicted using the state of the other one, but not the other way around, it means we have *generalized synchronization* [GS]. This means that there is a directional function connecting the responses of both systems, which is expressed as:

$$y(t) = \psi(x(t)), \tag{1.7}$$

Looking at the type of the analyzed system we can distinguish synchronization of externally forced periodic oscillators and synchronization of coupled oscillators. In the first case, the presence of synchronization is determined by the magnitude of forcing as well as by *detuning parameter*, representing the difference between natural frequency of the system and the frequency of the applied force. The basic example of coupled system is written as:

$$\frac{dx_1}{dt} = f_1(x_1) + \epsilon p_1(x_1, x_2) \tag{1.8}$$

$$\frac{dx_2}{dt} = f_2(x_2) + \epsilon p_2(x_1, x_2) \tag{1.9}$$

with ϵ being the coupling parameter, that ensures synchronization between the two systems. When coupling parameter tends to zero, the systems oscillate with their own natural frequencies.

In case of noisy systems, being intermittent systems between periodic and chaotic one, we can observe imperfect phase synchronization [IPS], for which frequencies nearly adjust and phase slips take place.

Synchronization is also possible to be observed in chaotic systems, but its detection is complex. In order to do this, one have to define the mean observed frequency of the system in terms of unstable periodic orbits, that are embedded in the chaotic attractor.

Chapter 2

Model of the system

The analyzed system is shown in Fig. 2.1. It consists of two identical elastic pendula of length l_0, spring stiffness k_2 and masses m, which are suspended on the oscillator. The oscillator consists of a bar, suspended on linear spring with stiffness k_1 and linear viscous damper with damping coefficent C_1. The system has five degrees of freedom. Mass M is constrained to move only in vertical direction and thus is described by the coordinate y. The motion of the first pendulum is described by angular displacement φ and its mass by coordinate x_2, that represent the elongation of the elastic pendulum. Similarly the second pendulum is described by angular displacement ϕ and its mass by coordinate x_3. Both pendulas are damped by torques with identical damping coefficent C_2, that depend on their angular velocities (not shown in Fig. 2.1). The small damping, with damping coefficient C_3 is also taken for pendula masses. The system is forced parametrically by vertically applied force $F(t) = F_0 \cos \nu t$, acting on the bar of mass M, that connects the pendula. F_0 denotes the amplitude of excitation and ν the excitation frequency.
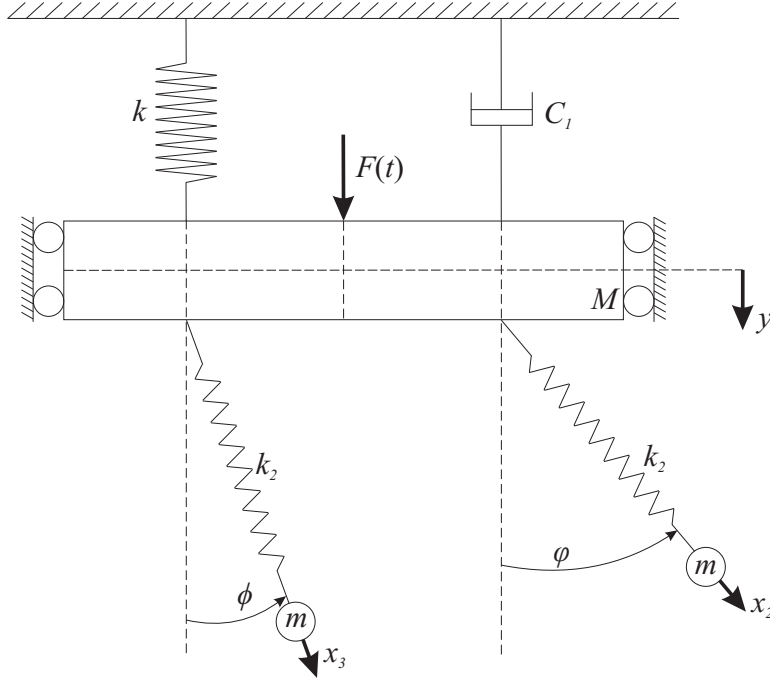
Figure 2.1: Model of the system

The equations of motion can be derived using Lagrange equations of the second type. The kinetic energy T, potential energy V, and Rayleigh dissipation D are given respectively by:

$$T = \frac{1}{2}(M + 2m)\dot{y}^2 + \frac{1}{2}m\dot{x}_3^2 + \frac{1}{2}m(l_0 + y_{wst2} + x_3)^2\dot{\phi}^2 + m\dot{y}\dot{x}_3\cos\phi + \qquad (2.1)$$

$$-m\dot{y}\dot{\phi}(l_0 + y_{wst2} + x_3)\sin\phi + \frac{1}{2}m\dot{x}_2^2 + \frac{1}{2}m(l_0 + y_{wst2} + x_2)^2\dot{\varphi}^2 +$$

$$+m\dot{y}\dot{x}_2\cos\varphi - m\dot{y}\dot{\varphi}(l_0 + y_{wst2} + x_2)\sin\varphi$$

$$V = -mg(l_0 + y_{wst2} + x_2)\cos\varphi - mg(l_0 + y_{wst2} + x_3)\cos\phi + \qquad (2.2)$$

$$mg(l_0 + y_{wst2}) + mg(l_0 + y_{wst2}) + \frac{1}{2}k_1(y + y_{wst1})^2 + \frac{1}{2}k_2(y_{wst2} + x_2)^2 +$$

$$+\frac{1}{2}k_2(y_{wst2} + x_3)^2 - (M + 2m)gy$$

$$D = \frac{1}{2}C_2\dot{\varphi}^2 + \frac{1}{2}C_2\dot{\phi}^2 + \frac{1}{2}C_3\dot{x}_2^2 + \frac{1}{2}C_3\dot{x}_3^2 \tag{2.3}$$

where C_3 is the damping coefficient of the pendulum mass and $y_{wst1} = \frac{(M+2m)g}{k_1}$, $y_{wst2} = \frac{mg}{k_2}$ represent static deflation of mass M and pendulums' mass m respectively. The system is described by five second order differential equations given in the following form:

$$m(l_0 + y_{wst2} + x_2)^2\ddot{\varphi} + 2m(l_0 + y_{wst2} + x_2)\dot{\varphi}\dot{x}_2 - m\ddot{y}(l_0 + y_{wst2} + x_2)\sin\varphi + \tag{2.4}$$

$$+mg(l_0 + y_{wst2} + x_2)\sin\varphi + C_2\dot{\varphi} = 0$$

$$m(l_0 + y_{wst2} + x_3)^2\ddot{\phi} + 2m(l_0 + y_{wst2} + x_3)\dot{\phi}\dot{x}_3 - m\ddot{y}(l_0 + y_{wst2} + x_3)\sin\phi + \tag{2.5}$$

$$+mg(l_0 + y_{wst2} + x_3)\sin\phi + C_2\dot{\phi} = 0$$

$$m\ddot{x}_3 + m\ddot{y}\cos\phi - m\dot{\phi}^2(l_0 + y_{wst2} + x_3) - mg\cos\phi + \tag{2.6}$$

$$+k_2(y_{wst2} + x_3) + C_3\dot{x}_3 = 0$$

$$m\ddot{x}_2 + m\ddot{y}\cos\varphi - m\dot{\varphi}^2(l_0 + y_{wst2} + x_2) - mg\cos\varphi + \tag{2.7}$$

$$+k_2(y_{wst2} + x_2) + C_3\dot{x}_2 = 0$$

$$(M + 2m)\ddot{y} + m\ddot{x}_3\cos\phi - 2m\dot{x}_3\dot{\phi}\sin\phi - m(l_0 + y_{wst2} + x_3)\ddot{\phi}\sin\phi + \tag{2.8}$$

$$-m(l_0 + y_{wst2} + x_3)\dot{\phi}^2\cos\phi + m\ddot{x}_2\cos\varphi - 2m\dot{x}_2\dot{\varphi}\sin\varphi +$$

$$-m(l_0 + y_{wst2} + x_2)\ddot{\varphi}\sin\varphi - m(l_0 + y_{wst2} + x_2)\dot{\varphi}^2\cos\varphi +$$

$$-(M + 2m)g + k_1(y + y_{wst1}) + C_1\dot{y} - F_0\cos\nu t = 0$$

In the numerical calculations we use the following values of parameters:

$$M = 10 \text{ [kg]}, \qquad m = 0.2 \text{ [kg]}, \qquad l_0 = 0.24849 \text{ [m]},$$

$$k_1 = 1642.3 \text{ } [\frac{N}{m}], \qquad k_2 = 19.7 \text{ } [\frac{N}{m}],$$

$$C_1 = 13.1 \text{ } [\frac{Ns}{m}], \qquad C_2 = 0.00776 \text{ [Nms]}, \qquad C_3 = 0.49 \text{ } [\frac{Ns}{m}],$$

$$y_{wst1} = 0.062 \text{ [m]}, \qquad y_{wst2} = 0.1 \text{ [m]}$$

Introducing dimensionless time $\tau = \omega_1 t$, where $\omega_1^2 = \frac{k_1}{M+2m}$ is the natural frequency of mass M with the attached pendulas, we obtain dimensionless equations of motion written as:

$$\ddot{\Psi} + \frac{2\beta_2}{(1 + y_{2st} + \chi_2)}\dot{\Psi}\dot{\chi}_2 - \frac{\beta_1^2}{(1 + y_{2st} + \chi_2)}\ddot{\gamma}\sin\Psi + \frac{\sin\Psi}{(1 + y_{2st} + \chi_2)} + \tag{2.9}$$

$$+ \frac{\alpha_2}{(1 + y_{2st} + \chi_2)^2}\dot{\Psi} = 0$$

$$\ddot{\Phi} + \frac{2\beta_2}{(1 + y_{2st} + \chi_3)}\dot{\Phi}\dot{\chi}_3 - \frac{\beta_1^2}{(1 + y_{2st} + \chi_3)}\ddot{\gamma}\sin\Phi + \frac{\sin\Phi}{(1 + y_{2st} + \chi_3)} + \tag{2.10}$$

$$+ \frac{\alpha_2}{(1 + y_{2st} + \chi_3)^2}\dot{\Phi} = 0$$

$$\ddot{\chi}_3 + \frac{\beta_1^2}{\beta_2^2}\ddot{\gamma}\cos\Phi - \frac{1 + y_{2st} + \chi_3}{\beta_2^2}\dot{\Phi}^2 - \frac{1}{\beta_2^2}\cos\Phi + y_{st2} + \chi_3 + \alpha_3\dot{\chi}_3 = 0 \tag{2.11}$$

$$\ddot{\chi}_2 + \frac{\beta_1^2}{\beta_2^2}\ddot{\gamma}\cos\Psi - \frac{1 + y_{2st} + \chi_2}{\beta_2^2}\dot{\Psi}^2 - \frac{1}{\beta_2^2}\cos\Psi + y_{st2} + \chi_2 + \alpha_3\dot{\chi}_2 = 0 \tag{2.12}$$

$$\ddot{\gamma} + \frac{\beta_2^2 a}{\beta_1^2}\ddot{\chi}_3\cos\Phi - \frac{2\beta_2 a}{\beta_1^2}\dot{\chi}_3\dot{\Phi}\sin\Phi - \frac{(1 + y_{2st} + \chi_3)a}{\beta_1^2}\ddot{\Phi}\sin\Phi + \tag{2.13}$$

$$- \frac{(1 + y_{2st} + \chi_3)a}{\beta_1^2}\dot{\Phi}^2\cos\Phi + \frac{\beta_2^2 a}{\beta_1^2}\ddot{\chi}_2\cos\Psi - \frac{2\beta_2 a}{\beta_1^2}\dot{\chi}_2\dot{\Psi}\sin\Psi +$$

$$-\frac{(1 + y_{2st} + \chi_2)a}{\beta_1^2}\ddot{\Psi}\sin\Psi - \frac{(1 + y_{2st} + \chi_2)a}{\beta_1^2}\dot{\Psi}^2\cos\Psi+$$

$$-\frac{1}{\beta_1^2} + \gamma + y_{1st} + \alpha_1\dot{\gamma} - q\cos\mu\tau = 0$$

where :

$$\omega_2^2 = \frac{k_2}{m}, \quad \omega_4^2 = \frac{g}{l_0}, \quad \mu = \frac{\nu}{\omega_1}, \quad y_{1st} = \frac{y_{wst1}}{l_0}, \quad y_{2st} = \frac{y_{wst2}}{l_0},$$

$$\beta_1 = \frac{\omega_1}{\omega_4}, \quad \beta_2 = \frac{\omega_2}{\omega_4}, \quad a = \frac{m}{M + 2m}, \quad q = \frac{F_0}{\omega_1^2 l_0(M + 2m)},$$

$$\alpha_1 = \frac{C_1}{\omega_1(M + 2m)}, \quad \alpha_2 = \frac{C_2}{m\omega_4 l_0^2}, \quad \alpha_3 = \frac{C_3}{m l_0 \omega_2^2},$$

$$\gamma = \frac{y}{l_0}, \quad \dot{\gamma} = \frac{\dot{y}}{l_0\omega_4}, \quad \ddot{\gamma} = \frac{\ddot{y}}{l_0\omega_4^2}, \quad \chi_3 = \frac{x_3}{l_0}, \quad \dot{\chi}_3 = \frac{\dot{x}_3}{l_0\omega_2},$$

$$\ddot{\chi}_3 = \frac{\ddot{x}_3}{l_0\omega_2^2}, \quad \chi_2 = \frac{x_2}{l_0}, \quad \dot{\chi}_2 = \frac{\dot{x}_2}{l_0\omega_2}, \quad \ddot{\chi}_2 = \frac{\ddot{x}_2}{l_0\omega_2^2}, \quad \Psi = \varphi,$$

$$\dot{\Psi} = \frac{\dot{\varphi}}{\omega_4}, \quad \ddot{\Psi} = \frac{\ddot{\varphi}}{\omega_4^2}, \quad \Phi = \phi, \quad \dot{\Phi} = \frac{\dot{\phi}}{\omega_4}, \quad \ddot{\Phi} = \frac{\ddot{\phi}}{\omega_4^2}$$

The dimensionless parameters of the system have the following values:

$$\beta_1 = 2, \quad \beta_2 = 1.58,$$

$$\alpha_1 = 0.1, \quad \alpha_2 = 0.01, \quad \alpha_3 = 0.1$$

$$a = 0.0192, \quad y_{1st} = 0.25, \quad y_{2st} = 0.4$$

Chapter 3

Simulation

3.1   Motivation

We study system (2.9-2.13) in order to detect possible synchronization ranges. There are two basic types of synchronous motion, which are depicted in Fig. 3.1(a,b). The pendulas can synchronize either in-phase or in anti-phase with each other, i.e., $\theta = \phi$ or $\theta = -\phi$. In both mentioned cases the forces acting in vertical direction on mass M are identical (there are no forces in horizontal direction), hence the energy transmitted between mass M and pendulas in in-phase and anti-phase motion is also identical. If there is an in-phase synchronization, the anti-phase also coexists in the same range of parameters. The accessibility of in-phase and anti-phase motion is governed only by initial conditions. The pendulas' masses are always synchronized in the in-phase with each other, i.e., $x_2 = x_3$. The anti-phase configuration of the masses is not observed ($x_2 = -x_3$) with the oscillating pendulas. The anti-phase synchronization of masses is possible when the pendulas are in equilibrium positions, then the sum of forces transmitted to mass M is equal to zero.
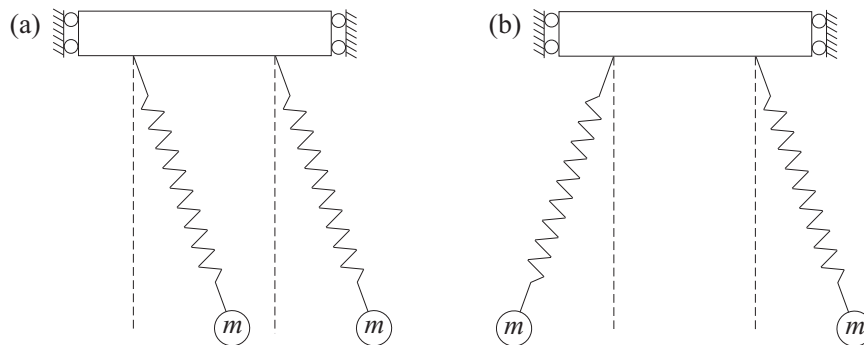
Figure 3.1: Possible synchronization (a) in phase, (b) in anti-phase

3.2 Free oscillations

As a first step to the understanding of the analyzed system free oscillations were considered. This means that the forcing in the system is set to 0. Moreover the damping in the pendula spring is neglected. As a result the following values of nondimensional parameters were used: $\beta_1 = 2$, $\beta_2 = 0.5$, $\alpha_1 = 0.1$, $\alpha_2 = 0.1$, $\alpha_3 = 0$, $a = 0.0192308$, $y_{1st} = 0.25$, $y_{2st} = 0.4$, $q = 0$. The analysis of free oscillations have shown, that it is possible to observe such state of the system, where pendula or pendula masses oscillate, and at the same time the bar M is stationary. Depending on the initial conditions, different configurations of such a behaviour are possible to be observed in the system. This includes for example anti-phase synchronization 1:1 of pendula masses, shown in Fig. 3.2. In that case, the pendula are displaced initially almost in anti-phase, which results in anti-phase 1:1 synchronization of pendula masses (Fig. 3.2(b)), whereas the pendula and bar M stop oscillating due to the damping, since the total force acting on the bar is zero. When the damping of the pendula motion is neglected ($\alpha_2 = 0$) we can observe similar behaviour with both pendula and pendula masses synchronizing. Fig. 3.3 presents the case, when after initial oscillations of pendula, pendula masses and the bar, finally 3.3(b&c) we observe anti-phase synchronization 1:1 of pendula and in-phase synchronization 1:1 of pendula masses. Fig. 3.3(d&e) show synchronization graphs for pendula and pendula masses respectively. In Fig. 3.4(b&c) we see example of a *quarter synchronization* of pendula (shifted by quarter of a period), as defined by Czołczyński *et. al.* [4] and anti-phase synchronization of pendula masses. In both these cases at first pendula masses oscillate in phase, with increasing amplitudes, that decrease as the motion stabilizes and final configuration is reached.
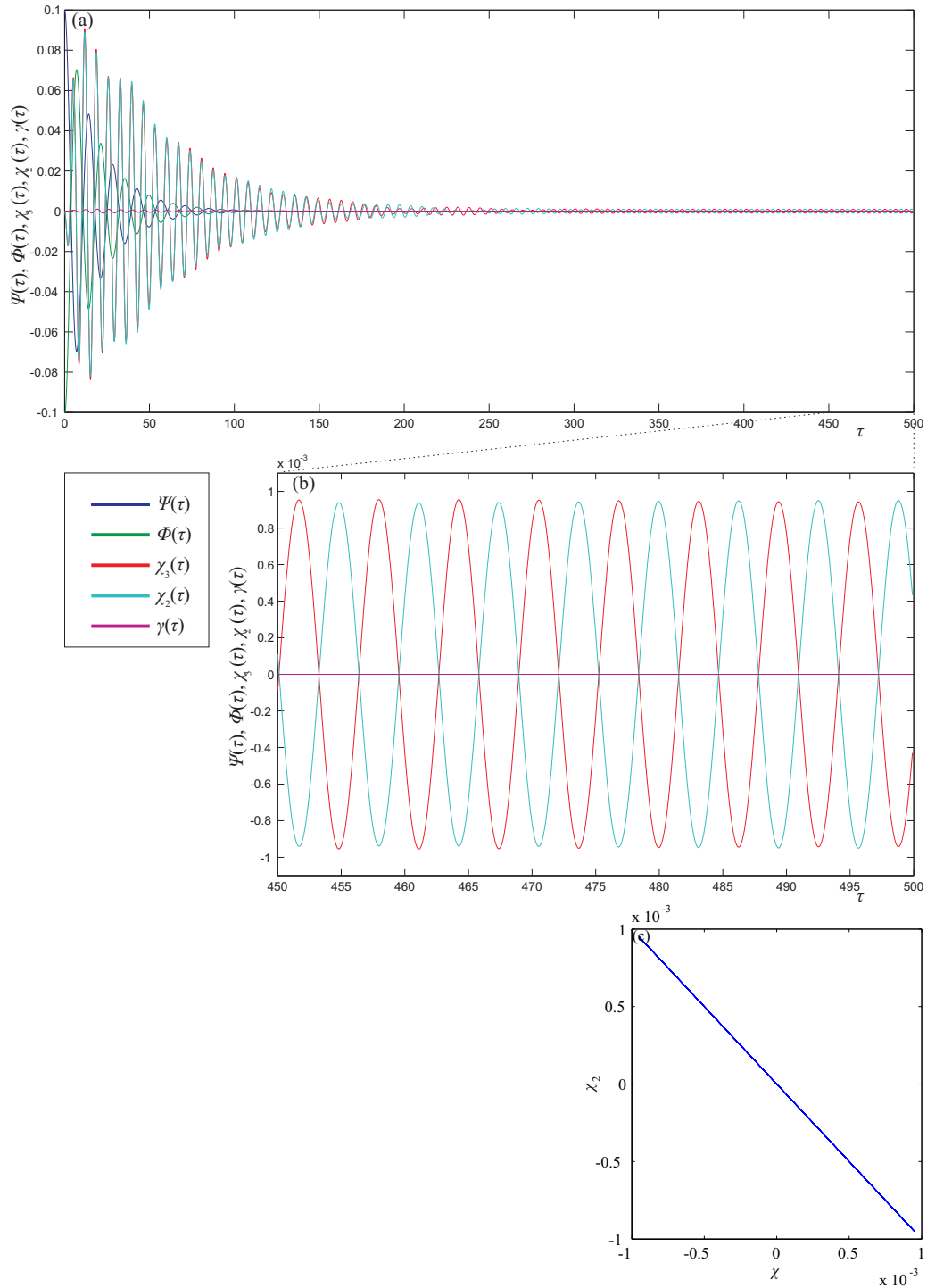
Figure 3.2: (a) & (b) Free oscillations corresponding to coordinates Ψ, Φ, χ_3, χ_2, γ, for nonzero initial conditions: $\Psi(0) = 0.1$, $\Phi(0) = -0.101$, (c) synchronization graph for the pendula masses as depicted in (b)

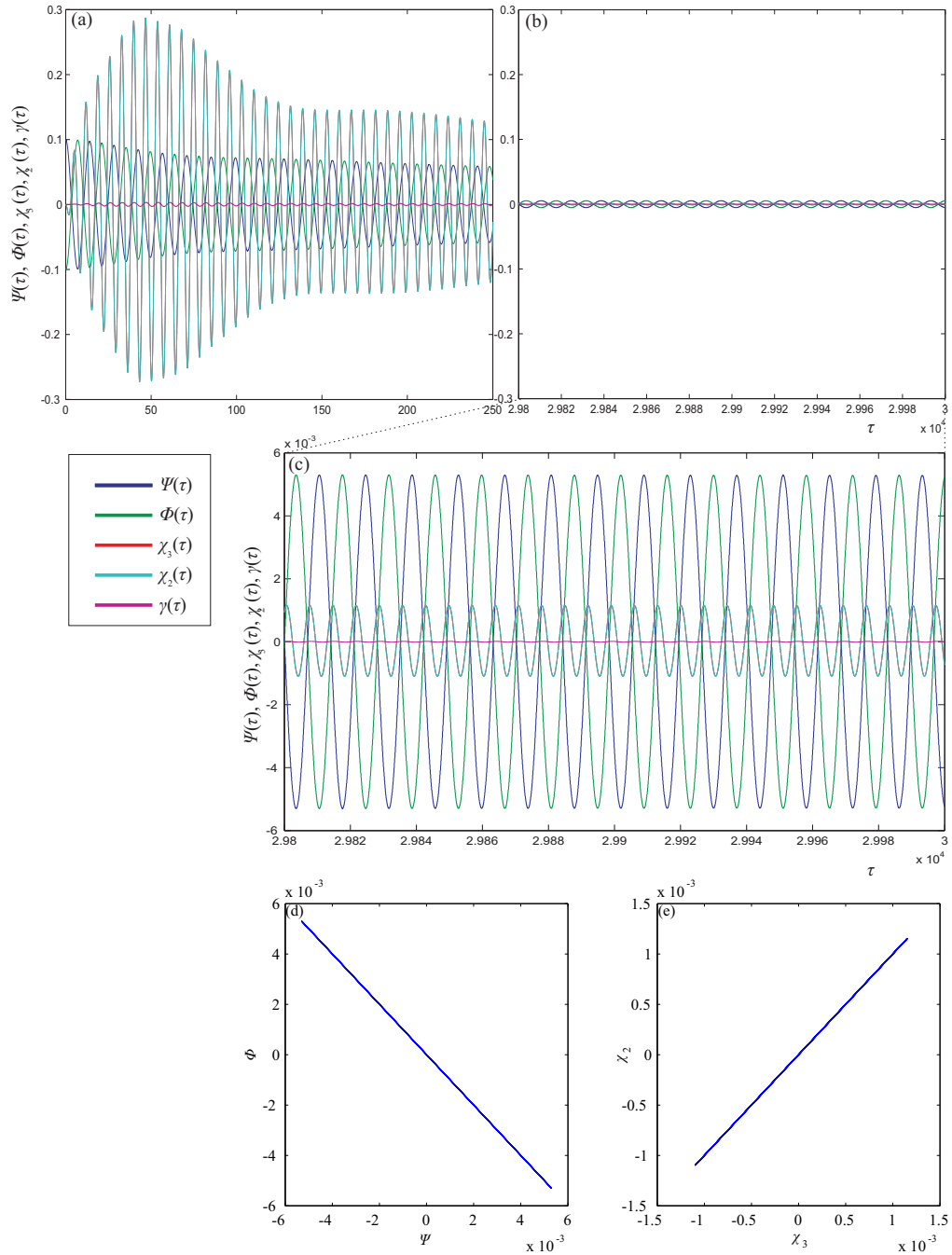Figure 3.3: (a) & (b) & (c) Free oscillations corresponding to coordinates Ψ, Φ, χ_3, χ_2, γ, with pendula damping set to $\alpha_2 = 0$ and nonzero initial conditions: $\Psi(0) = 0.1$, $\Phi(0) = -0.1$, (d) &(e) synchronization graphs for the pendula and pendula masses respectively, as depicted in (c)
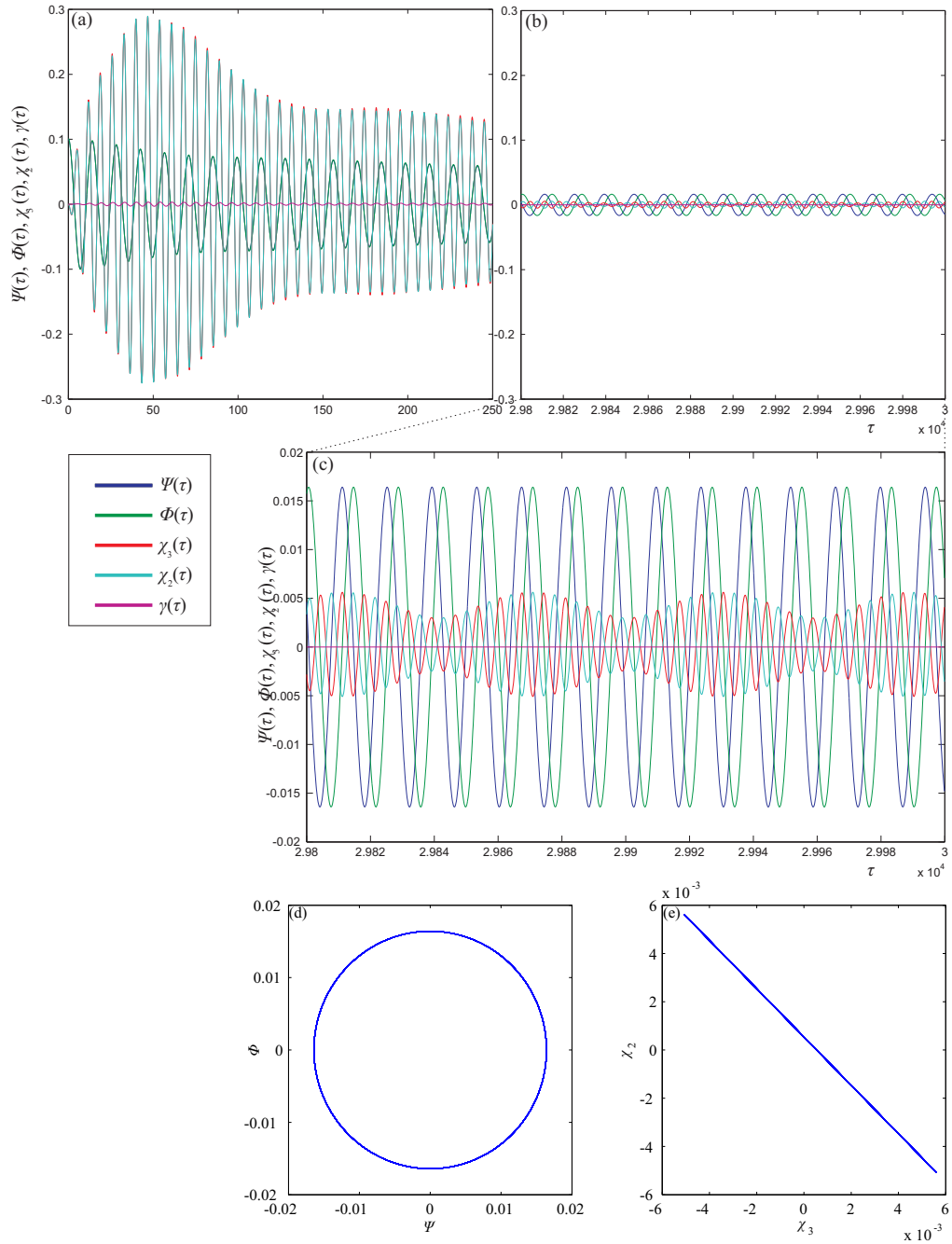
Figure 3.4: (a) & (b) & (c) Free oscillations corresponding to coordinates Ψ, Φ, χ_3, χ_2, γ, with pendula damping set to $\alpha_2 = 0$ and nonzero initial conditions: $\Psi(0) = 0.1$, $\Phi(0) = 0.101$, (d) &(e) synchronization graphs for the pendula and pendula masses respectively, as depicted in (c)
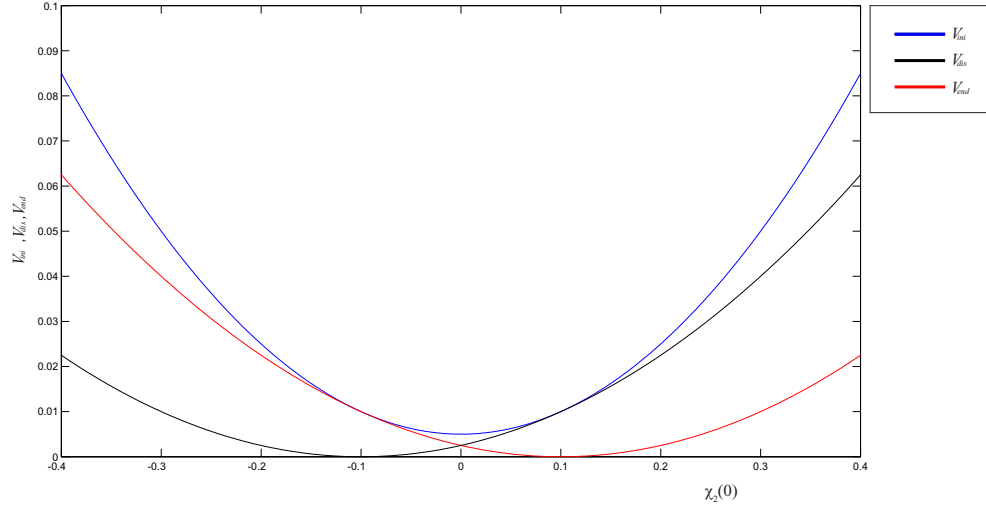
Figure 3.5: Potential energies :V_{ini}, V_{end}, V_{dis} as a function of initial condition $\chi_2(0)$, for other nonzero initial condition: $\chi_3(0) = 0.1$

Fig. 3.5 illustrates the dependence of initial potential energy V_{ini}, end potential energy V_{end} and dissipated energy V_{dis} on the initial condition of pendula mass $\chi_2(0)$. It clearly confirms that we can find appropriate initial condition for this mass, so that the energy dissipated in the system would be zero. This type of analysis allows us to clearly determine the necessary initial conditions, so that the described behaviour could be observed.

3.3   Stability of synchronous motion

In this section we study the stability of the observed synchronous oscillations and rotations of the pendula. We present the bifurcation diagrams calculated in two-parameter space: amplitude q versus frequency μ of excitation. We focus our attention on determining the regions of synchronous stable motion and bifurcations that lead to their destabilization. We consider the state of the system in the following range $q \in [0, 1.2]$ of forcing amplitudes and frequency of excitation belonging to the range $\mu \in [0.3, 1.2]$, which cover the possible resonances in the system. Resonance should be observed when the frequency of excitation comes close to the natural frequencies: of mass M $\mu_M = 1$, of pendula $\mu_p \approx 0.50$ and pendulum mass $\mu_{pm} \approx 0.79$. Fig. 3.6 presents two parameter bifurcation diagram, obtained by direct integration. It shows the existence of synchronous, asynchronous motion and equilibrium solutions. As soon as we have a lot of coexisting solutions to hold clearance of Figure 3.6 we do not distinguish which type of synchronous or asynchronous we find. For low amplitudes of excitation, the only solution is equilibrium, which turns into synchronous or asynchronous solution as the frequency of excitation increases. The detailed

analysis of synchronous solutions was performed using continuation software Auto-07p [6]. We calculate the stability borders of each identified case, i.e., the ranges inside which the given motion is stable. The first periodic solution is observed for frequency of excitation around $\mu \approx 0.4$ and for amplitudes of excitation above $q \approx 0.8$. This periodic solution shown in Fig. 3.7(a) is identified as anti-phase oscillations of pendula and pendula masses locked 1:1 with forcing. This solution is destabilized by Saddle-Node bifurcation curve (green line), period doubling (blue line) and Neimark-Sacker (red line) bifurcations. The continuation reveals that for small range of parameters, around the frequency of excitation close to the natural frequency of pendula, this solution coexists with in-phase 2:1 oscillations. Oscillations 2:1 are destabilized by Saddle-Node bifurcation curve then by Neimark-Sacker and pitchfork symmetry breaking bifurcation (SB2). In the investigated system we distinguish two different symmetry breaking pitchfork bifurcations one of them (SB2) brokes symmetry between the pendulas, the second one (SB1) brokes the symmetry of each pendula but their motion remains identical. As the frequency of excitation increases we observe either asynchronous motion or equilibrium. With further increase of excitation frequency we observe asynchronous behavior, which change into two small regions of in-phase rotations 3:1. We show it in Fig. 3.7(f) and this area is bounded by Neimark-Sacker, period doubling and Saddle-Node bifurcations. This solution coexists with rotations in phase 2:1, presented also in Fig. 3.7(f). The stability region for this solution is bounded by pitchfork SB1 bifurcation from the left and right, Neimark-Sacker from above, and Saddle-Node and Neimark-Sacker bifurcations from the right. Both these solutions coexist in small range of considered parameters with another synchronous anti-phase rotations 4:1, presented in Fig. 3.7(f). The synchronous motion destabilizes from the right by Saddle-Node and pitchfork SB2 curves, from above by Neimark-Sacker, and from the left by Neimark-Sacker, Saddle-Node and pitchfork SB2 curves.

Around $\mu \approx 0.8$, where the resonance of pendulum masses occur, the system possesses quite rich dynamics, which results in the coexistence of different synchronous solutions together with asynchronous solutions. This includes anti-phase rotations 2:1 depicted in Fig. 3.7(c,d) , in-phase rotations 1:1 shown in Fig. 3.7(b), in-phase 3:1 rotations of pendula and pendula masses 3:1 presented in Fig. 3.7(e). Thereby it is not possible to fully compare the bifurcation diagram from the direct integration with the results from Auto-07p. In the case of rotations 2:1 the synchronous motion is destroyed from the right by Saddle-Node and pitchfork SB2 curves, from above by Neimark-Sacker, and from the left by Saddle-Node, Neimark-Sacker and pitchfork SB2 bifurcations. Rotations 1:1 are destabilized by pitchfork SB2 from the right, and by Neimark-Sacker and period doubling from the left. The rotations 3:1 are mainly destabilized by pitchfork SB2 from the right and by pitchfork SB2 and period doubling from the bottom, and by period dou-

bling, pitchfork SB2, Saddle-Node and Neimark-Sacker from the left. From this solution, through period-doubling bifurcation we find synchronized rotations 6:1-6:1, shown in Fig. 3.7(e). This solution is destabilized from above by period-doubling bifurcation, from the left through pitchfork SB2 bifurcation, and from below through Saddle-Node bifurcation (not visible, since coincides with period-doubling boundary for rotations 3:1-3:1).

As we pass through the resonance frequency of mass M $\mu = 1$, for higher amplitudes of excitation the only synchronous solution includes anti-phase 2:1 rotations depicted in Fig. 3.7(c,d) . After the resonance, for amplitudes of excitation above $q \approx 0.12$, only asynchronous solutions are observed. Below this value, many small synchronous regions were found. This includes in-phase 1:1 oscillations and two regions of in-phase 2:1 oscillations, together with two regions of in-phase 2:1 rotations. The region of 1:1 oscillations is enclosed by Saddle-Node, Neimark-Sacker and pitchfork SB2 bifurcation curves. Oscillatory 2:1 motion destabilizes through pitchfork SB1 from above and Neimark-Sacker curves from below. This solution coexists for small range of parameters with 2:1 rotations, which motion is destabilized by period doubling and Neimark-Sacker from the left, and from the right by pitchfork SB2, Neimark-Sacker and period doubling curves. We observe the excellent correlation in these regions between the results from numerical continuation and direct integration.
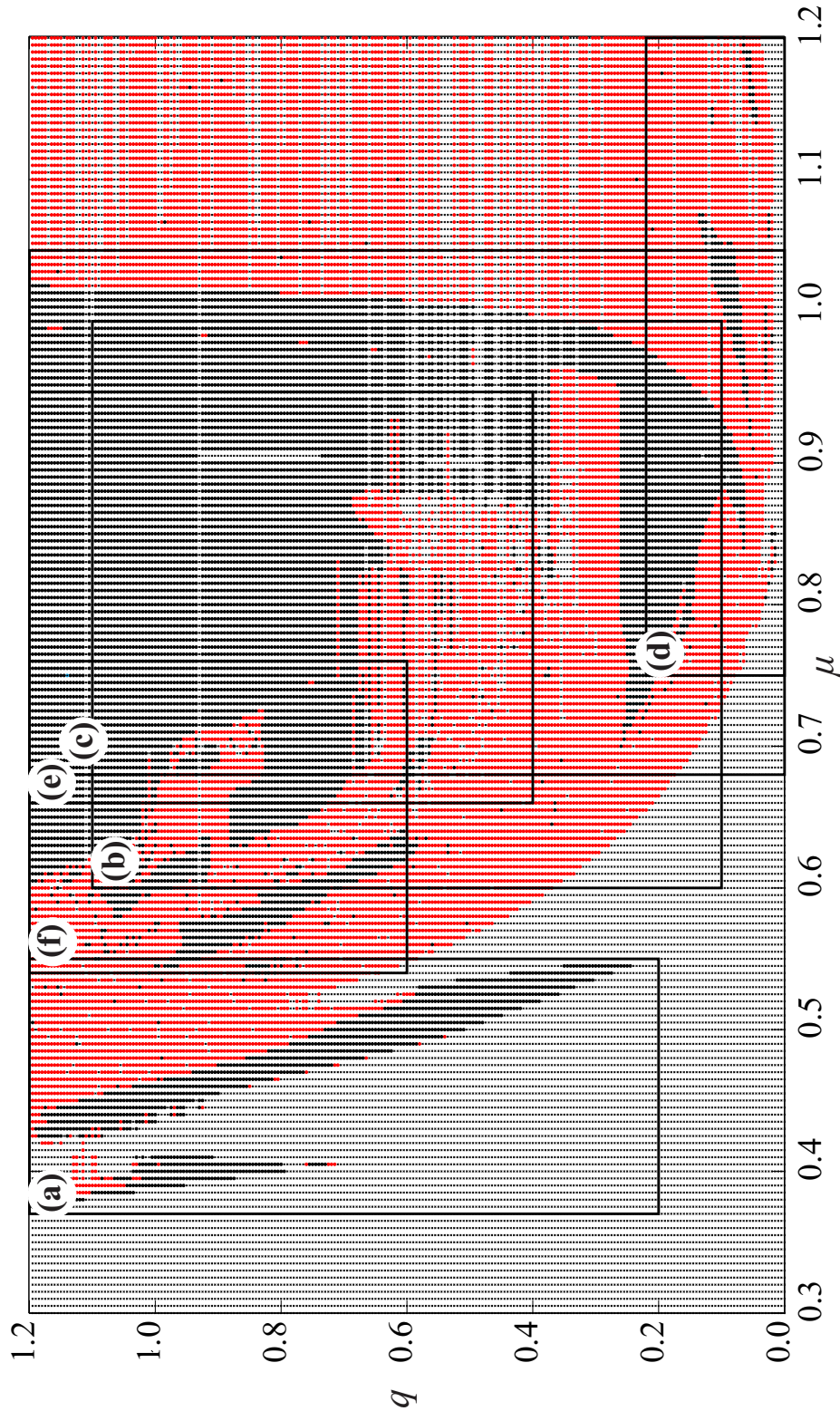
Figure 3.6: The synchronous (red dots), asynchronous (black dots) and equilibrium (small black crosses) solutions of system (9-13) in two parameters space: μ frequency and q amplitude of excitation. We calculate this plot by direct integration using 4th order Runge-Kutta algorithm. In rectangles (a-f) we highlighted regions of synchronous motion calculated in Auto-07p (see Fig. 3.7)
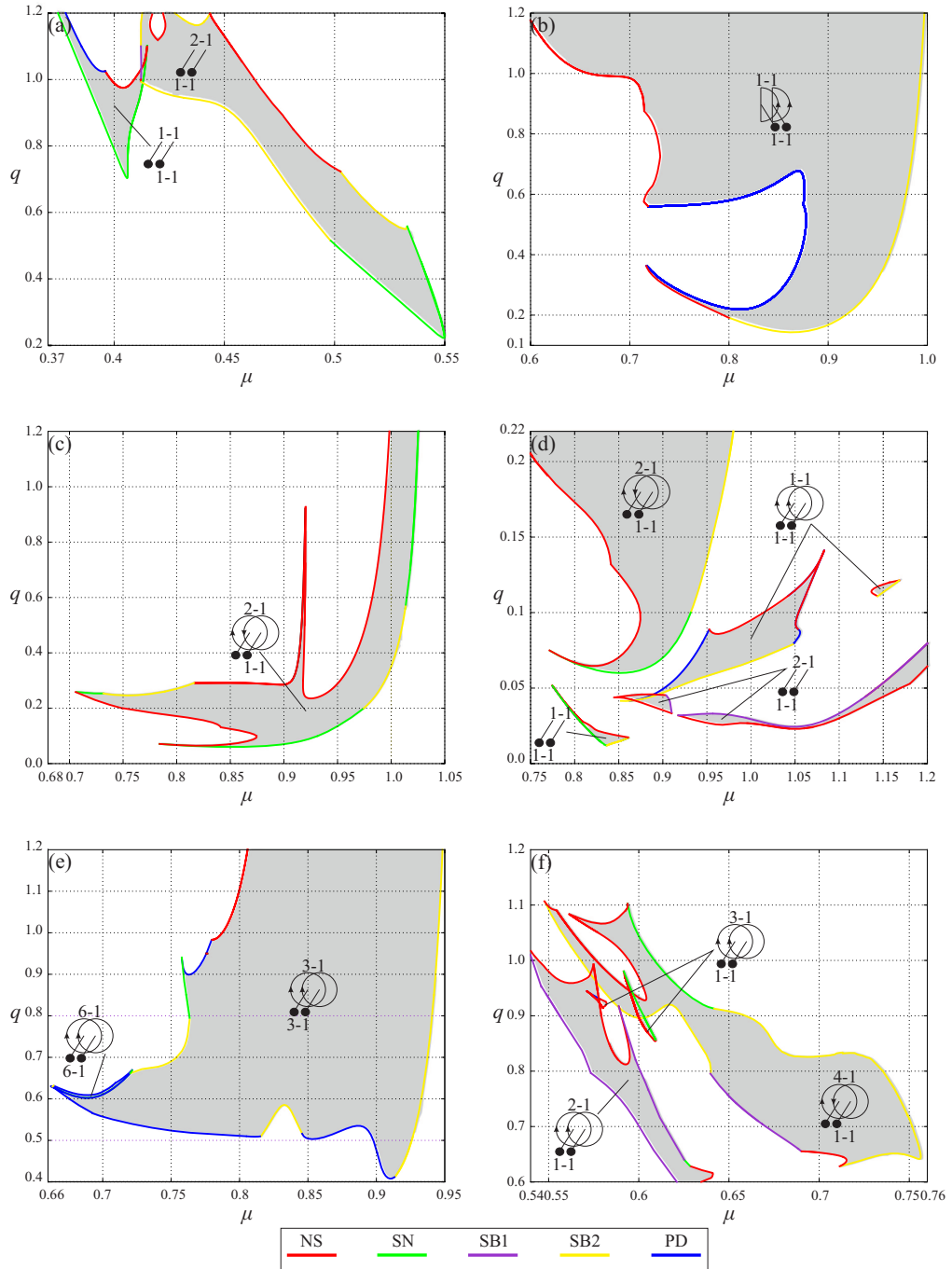
Figure 3.7: Stable ranges of synchronous motion calculated in Auto-07p (see rectangles in Fig. 3.6). Color of lines stand for different types of bifurcation: Neimark-Sacker (red), Saddle-Node (green), pitchfork SB1 (violet), pitchfork SB2 (yellow) and period doubling (blue). In region inside lines synchronous solutions are periodic and stable.

3.4   1 parameter continuation

In this subsection we show one parameter continuation for four periodic solutions (two oscillating and two rotational), as a bifurcation parameter we choose the frequency of excitation. In Figure 3.8 (a-d) we present the synchronized oscillating periodic solutions, their regions of stability are shown in Fig. 3.7 (a). Considered system (2.9-2.13) given by five second order ODEs, hence we have ten dimensional phase space and at least five figures (amplitude of each degree) show its complete dynamics. To decrease it we focus on the dynamics of one pendula (the second pendula has the same amplitude in the synchronized state) and mass M. The first presented periodic solutions in Fig. 3.8(a,b) is antiphase 2:1-1:1 oscillations, in previous subsection we show that this solution is destabilized by Neimark-Sacker bifurcation from the right and from the left by pitchfork symmetry braking SB2. Changing the branch at pitchfork bifurcation enables us to find another stable periodic branch of asynchronized oscillations 2:1-1:1, that looses its stability through the Saddle-Node bifurcation. After pitchfork symmetry breaking SB2 bifurcation the solution of one pendulum is located at upper branch (see Fig. 3.8(b)) and the second pendulum on lower branch or vice-versa. The periodic oscillations 2:1-1:1, shown in Fig. 3.8 (c,d), present much richer scenario than other solutions. These oscillations destabilize from both sides through pitchfork SB2 bifurcation. When we switch branch in left SB2 point, we find periodic stable solution of asynchronized oscillations 2:1-1:1 when the amplitudes of pendulas reach zero their motion stops and in the opposite direction the stability is lost in pitchfork SB2 bifurcation. Another change of branch allows us to observe another asynchronous periodic solution, for which pendulum 1 oscillates 2:1, pendulum 2 is at rest (not shown here) and pendula masses oscillate 1:1 in asynchronized manner. One end of this stable solution destabilizes through Saddle-Node bifurcation and the second one by pitchfork SB2 bifurcation. As the frequency of excitation increases the stability of this solution is regained through pitchfork SB2 bifurcation and lost again through Saddle-Node bifurcation. Note that for the mass M, the bifurcation points that are responsible for the destabilization of periodic solutions for synchronized in-phase oscillations 2:1-1:1 and nonsynchronized oscillations 2:1-1:1, are placed very close to each other. When we switch the branch in the right SB2 bifurcation point of the synchronized in-phase oscillations 2:1-1:1, we find asynchronized solution of oscillations 2:1-1-1 that persists for small interval of frequency of excitation. It destabilizes from above and below through period-doubling bifurcation points. Switching the branch in lower PD point enables us to observe non-synchronized oscillations 4:1-2:1, that destabilize through Neimark-Sacker bifurcation. The bifurcation diagram, shown in Fig. 3.9 (a-b), shows 3:1-3:1 rotational periodic solutions for $q = 0.654$. In contary to the previous cases on the horizontal axis we plot the velocity amplitude (to hold a physical meaning). The stability region of this

solution is shown in Fig. 3.7 (e) This solution looses its stability through period-doubling and pitchfork SB2 bifurcation. Switching the branch in the period-doubling bifurcation point, allows to observe cascade of period doublings, which lead us to two branches of synchronized periodic 6:1-6:1 rotational solution, that looses its stability through period-doubling bifurcation. When we switch branch in these PD points, we reach two branches of synchronized periodic 12:1-12:1 rotational solutions. They are stable through very small range of frequency of excitation, loosing stability as a result of Neimark-Sacker bifurcation. After switching the branch in right pitchfork SB2 bifurcation point, we observe asynchronized rotations 3:1-3:1, that are stable in very small interval, finally loosing its stability through Saddle-Node bifurcation. Finally we show in Fig. 3.9 (c-d) synchronized rotations 4:1-1:1, that loose stability through pitchfork symmetry braking from the right and left. Switching the branch in both SB2 bifurcation points allows us to find asynchronous rotations 4:1-4:1, that are stable in very small interval of frequency of excitation, loosing finally stability through Saddle-Node bifurcation.
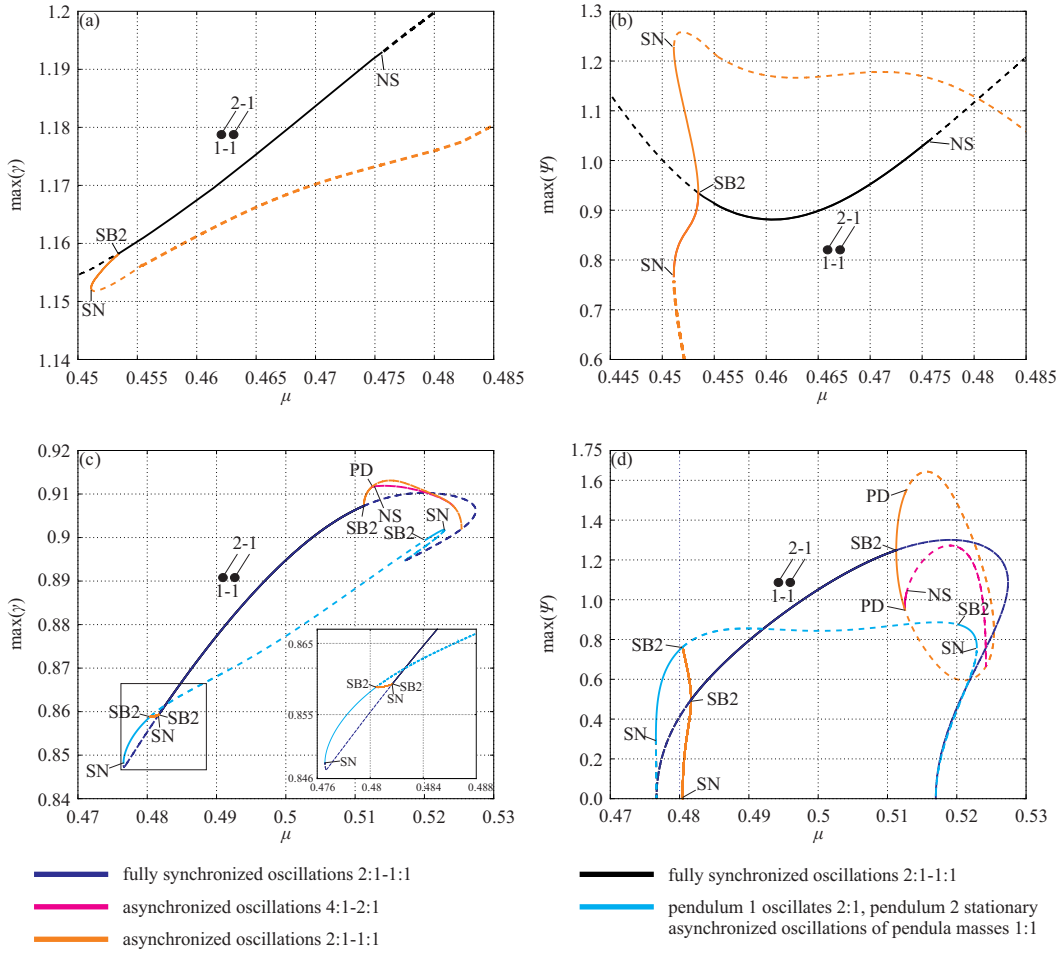
Figure 3.8: 1 parameter continuation of fully synchronized: 2:1-1:1 oscillations ((a) mass M, (b) pendulum 1, $q = 0.899$, $\mu = 0.455$), 2:1-1:1 oscillations ((c) mass M, (d) pendulum 1, $q = 0.654$, $\mu = 0.5$),
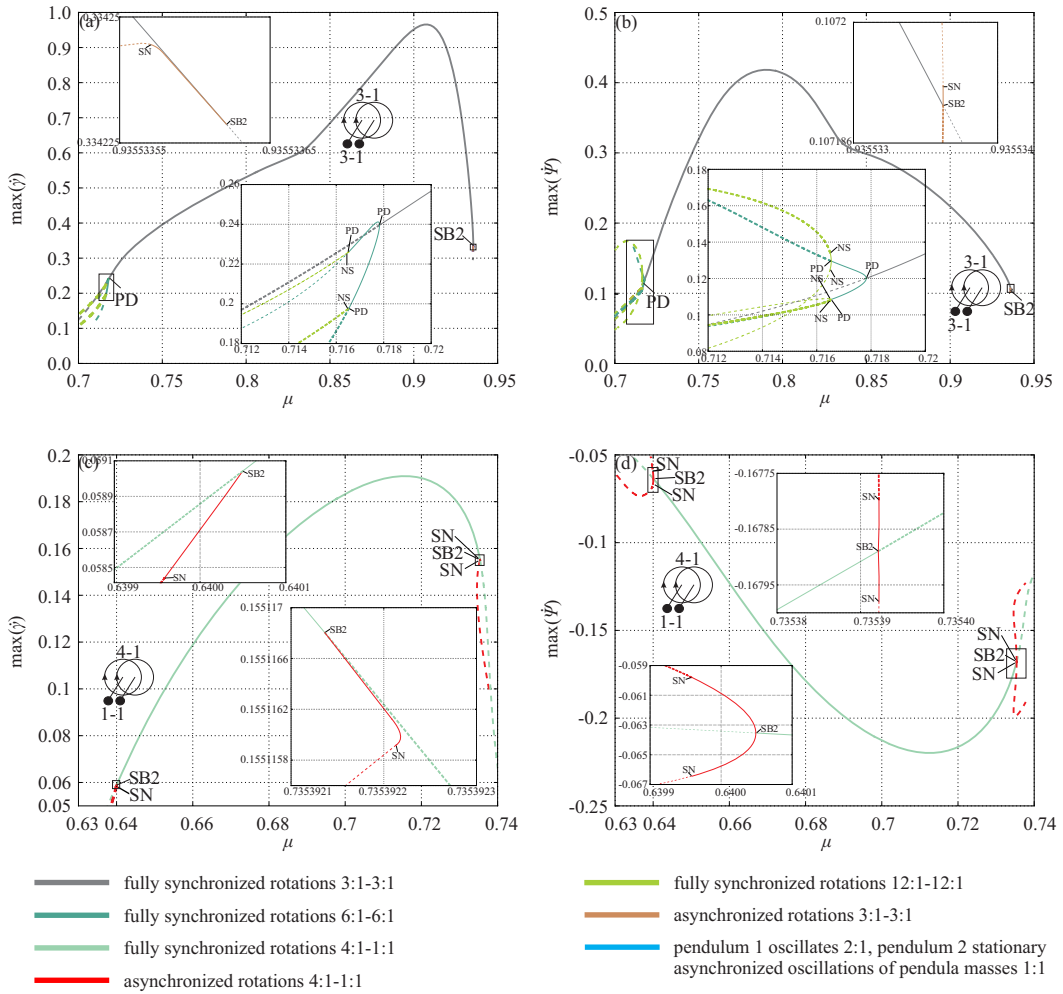
Figure 3.9: 1 parameter continuation of fully synchronized: 3:1-3:1 rotations ((a) mass M, (b) pendulum 1,$q = 0.654$, $\mu = 0.8$), 4:1-1:1 rotations ((c) mass M, (e) pendulum 1,$q = 0.8$, $\mu = 0.7$)

Chapter 4

Conclusions

In the system of two planar elastic pendula suspended on the excited linear oscillator one can observe both in-phase and anti-phase synchronization pendula. In-phase and anti-phase synchronous states always co-exist. Pendula can synchronize during the oscillatory and rotational motion but only when their behavior is periodic. We have not observed the synchronization of the chaotically behaving pendula. This result is contrary to the great number of chaos synchronization examples [17, 16, 9] but confirms the results obtained in [3] where it has been shown that the forced Duffing's oscillators mounted to the elastic beam can synchronize only after becoming periodic. The synchronization of the chaotic motion of the pendula is impossible as the excited oscillator transfers the same signal to both pendula which cannot differently modify the pendula's motion. We also have not observed in-phase or anti-phase synchronization of the pendula when masses m_2 and m_3 are in anti-phase. In this case the pendula in-phase or anti-phase synchronization is impossible as the pendula have different lengths.

We show two dimensional bifurcation diagrams with the most representative periodic solutions in the considered system. In the neighborhood of the linear resonances of subsystems we have rich dynamics with both periodic and chaotic attractors. Our results are robust as they exit in the wide range of system parameters, especially two dimensional bifurcation diagram can be used as a scheme of bifurcations in the class of systems similar to investigated in this thesis.

Bibliography

[1] B.A. Anicin, D.M. Davidovic, and V.M. Babovic. On the linear theory of the elastic pendulum. *European Journal of Physics*, 14:132–135, 1993.

[2] S. Boccaletti. The synchronized dynamics of complex systems. *Elsevier*, 2008.

[3] K. Czolczynski, T. Kapitaniak, P. Perlikowski, and A. Stefanski. Periodization of duffing oscillators suspended on elastic structure: Mechanical explanation. *Chaos Solitons & Fractals*, 32:920–926, 2007.

[4] K. Czolczynski, P. Perlikowski, A. Stefanski, and T. Kapitaniak. Synchronization of pendula rotating in different directions. *Communications in Nonlinear Science and Numerical Simulation*, 17(9):3658 − 3672, 2012.

[5] D.M. Davidovic, B.A. Anicin, and V.M. Babovic. The libration limits of the elastic pendulum. *American Journal of Physics*, 64(3), 1996.

[6] E.J. Doedel, B.E. Oldeman, A.R. Champneys, F. Dercole, T. Fairgrieve, Y. Kuznetsov, R. Paffenroth, B. Sandstede, X. Wang, and C. Zhang. *AUTO-07P: Continuation and Bifurcation Software For Ordinary Differential Equations*. Concordia University, Montreal, Canada, 2011.

[7] P. Lynch. Resonant motions of the three dimensional elastic pendulum. *International Journal of Non-Linear Mechanics*, 37:345–367, 2002.

[8] P. Lynch. The swinging spring: a simple model of atmospheric balance. 2002. In Norbury J., Roulstone I.(Eds.): Large-scale Atmosphere-Ocean Dynamics, Vol.II, Geometric Methods and Models, Cambridge University Press, Cambridge, pp. 64-108.

[9] Y. Maistrenko, T. Kapitaniak, and P. Szuminski. Locally and globally riddled basins in two coupled piecewise-linear maps. *Physical Review E*, 56:6393–6399, 1997.

[10] A. Najdecka and M. Wiercigroch. Rotational motion synchronization of parametric pendulums. *submitted to Physica D*. draft.

[11] H.N. Nunez-Yepez, A. L. Salas-Brito, C.A. Vargas, and L. Vicente. Onset of chaos in an extensible pendulum. *Physics Letters A*, 145(2,3), 1990.

[12] L. M. Pecora and T. L. Caroll. Synchronization in chaotic systems. *Physical Review Letters*, 64(8), 1990.

[13] A. Pikovsky, M. Rosenblum, and J. Kurths. *Synchronization: a universal concept in nonlinear sciences*. Cambridge University Press, 2001.

[14] D. Sado. *Drgania regularne i chaotyczne w wybranych ukladach z wahadlami*. WNT, Warszawa, 2010.

[15] C. Schafer, M.G. Rosenblum, J. Kurths J., and H.-H. Abel. Heartbeat synchronized with ventilation. *Nature*, 392:239, 1998.

[16] A. Stefanski and T. Kapitaniak. Using chaos synchronization to estimate the largest lyapunov exponent of nonsmooth systems. *Discrete Dynamics in Nature and society*, 4:207–215, 2000.

[17] A. Stefanski and T. Kapitaniak. Estimation of the dominant lyapunov exponent of non-smooth systems on the basis of maps synchronization. *Chaos Solitons & Fractals*, 15:233–244, 2003.

[18] A. Vitt and G. Gorelik. Oscillations of an elastic pendulum as an example of the oscillations of two parametrically coupled linear systems. *Journal of Technical Physics*, 3(2-3):294–307, 1933. Translated from Russian by Lisa Shields with an introduction.